

Article

Analysis of Observations near the Fourth Electron Gyrofrequency Heating Experiment in EISCAT

Zeyun Li, Hanxian Fang ^{*}, Hongwei Gong and Zhe Guo

College of Meteorology and Oceanography, National University of Defense Technology, Changsha 410073, China; lizeyun@nudt.edu.cn (Z.L.); gonghongwei18@nudt.edu.cn (H.G.); guozhe18@nudt.edu.cn (Z.G.)

* Correspondence: fanghx@hit.edu.cn

Abstract: We present the observations of the artificial ionospheric heating experiment of EISCAT (European Incoherent Scatter Scientific Association) on 22 February 2012 in Tromsø, Norway. When the pump is operating near the fourth electron gyrofrequency, the UHF radar observation shows some strong enhancements in electron temperature, electron density, ion line, and the outshifted plasma lines. Based on some existing theories, we find the following: first, Langmuir waves scattering off lower hybrid density fluctuations and strong Langmuir turbulence (SLT) in the Zakharov model cannot completely explain the outshifted plasma lines, but the data suggest that this phenomenon is related to the cascade of the pump wave and should be researched further; second, the spatiotemporal consistency between the enhancement in electron density/electron temperature reaches up to three to four times that of the undisturbed state and HF-enhanced ion lines (HFILs) suggest that SLT excited by parametric instability plays a significant role in superthermal electron formation and electron acceleration; third, some enhancements in HFILs and HF-induced plasma lines (HFPLs) are generated by parametric decay instability (PDI) during underdense heating in the third cycle, we suggest that this is due to the existence of a second cut-off in the upper hybrid dispersion relation as derived from a kinetic description.

Keywords: heating ionosphere; plasma line; electron temperature; electron density



Citation: Li, Z.; Fang, H.; Gong, H.; Guo, Z. Analysis of Observations near the Fourth Electron Gyrofrequency Heating Experiment in EISCAT. *Universe* **2021**, *7*, 191. <https://doi.org/10.3390/universe7060191>

Academic Editor:
Vladislav Demyanov

Received: 23 April 2021
Accepted: 4 June 2021
Published: 8 June 2021

Publisher's Note: MDPI stays neutral with regard to jurisdictional claims in published maps and institutional affiliations.



Copyright: © 2021 by the authors. Licensee MDPI, Basel, Switzerland. This article is an open access article distributed under the terms and conditions of the Creative Commons Attribution (CC BY) license (<https://creativecommons.org/licenses/by/4.0/>).

1. Introduction

The interaction of high-power high-frequency (HF) waves (usually termed as a pump) with the ionosphere can excite a series of complex phenomena due to parametric instability. According to the different excitation height, parametric instability can be divided into Langmuir parametric instability and thermal (resonance) parametric instability (TPI). In the process of TPI, the maximum wave-plasma interaction occurs in the double resonance regime, and double resonance exists in the ionosphere when the heating frequency f_{HF} , the upper hybrid frequency f_{UH} and the electron gyrofrequency match the following condition: $f_{HF} = f_{UH} = n f_{ce}$ ($n = 2, 3, 4, 5, 6$, and even greater, depending on the maximum electron concentration in this layer), where $f_{UH} = \sqrt{f_{plasma}^2 + f_{ce}^2}$ is the ionospheric plasma frequency and f_{ce} is the electron gyrofrequency at the altitude of the upper hybrid resonance h_{UH} [1,2]. Brodin and Stenflo [3] researched the resonant interaction between one upper hybrid wave and two electron Bernstein waves (with frequencies $\simeq 2f_{ce}$) in a uniform electron plasma. They used kinetic theory to calculate the coupling coefficient and growth rate in the process of three-wave interaction. The results showed that the coupling is especially strong in the plasma layer where $f_{ce}/f_{plasma} = 1/\sqrt{15}$. As the high-power HF O-mode radio waves reach the regions of their resonant interactions, complex phenomena arise, e.g., HF-enhanced ion lines (HFILs) and HF-induced plasma lines (HFPLs), an increase in electron temperature, and the perturbation of electron density. Many heating experiments have been conducted to research the effect of the pump frequency near a frequency that is a multiple of the electron gyrofrequency. Mjølhus et al. predicted that

the effect of ionospheric heating should be suppressed when the pump frequency was slightly below a harmonic of the electron gyrofrequency [4]. Honary et al. [5] found that the pump could not excite the small-scale field-aligned irregularities as pump frequencies approached the third electron gyrofrequency but induce very small-scale irregularities, which were responsible for the production of fast electrons and the ionized patches. The results given by Robinson et al. [6] indicate that there are strong minima in the responses of both anomalous absorption and electron temperature when pump frequency is operating in the vicinity of the third and fourth electron gyrofrequencies and that anomalous electron heating in the presence of small scale field aligned plasma irregularities dominates over collisional heating at high latitudes. Borisova et al. [7] also found that the small-scale field-aligned irregularities are suppressed near the fourth electron gyrofrequency. This effect is a typical feature for electron temperature during frequency-stepping experiments around $n f_{ce}$, and Mjølhus et al. proposed that this feature is related to the second cut-off in the upper hybrid dispersion relation as derived from a kinetic description [4].

In addition, the High-frequency Active Auroral Research Program (HAARP) heating facility near Gakona provides sufficient power to produce artificial ionospheric ionization [8]. The creation of artificial plasma layers near $2f_{ce}$ is optimized for f_{HF} slightly below the double resonance $2f_{ce} = f_{UH}$. Sergeev et al. observed that descending layers (DL) appear only during injections along the magnetic field at $f_{HF} > 4f_{ce}$ at the nominal interaction altitude in the background ionosphere at the HAARP facility [9]. For the same circumstances, Dhillon and Robinson reported descending ion line echoes when $f_{HF} > 5f_{ce}$ at EISCAT [10]. However, Ashrafi et al. and Mishin et al. reported on DL generation for heating both above and below $3f_{ce}$ and $4f_{ce}$ at different beam angles with distinct differences in descent speed and amplitude of the ionization layer power [11,12]. Kuo et al. reported that energetic electrons cause impact ionizations and descend to form artificial ionization layers at the bottom of the ionospheric F region [13]. Mishin et al. indicated that the generation of an artificial ionospheric layer may be related to strong Langmuir turbulence (SLT) [12]. Borisova et al. presented data of the pump frequency near the fifth electron gyrofrequency, including (1) electron temperature and electron density that vary with pump frequency; (2) a weak suppression of artificial ionospheric irregularities with transverse scales of 7.5–9.0 m during heating at a frequency near the fifth electron gyroharmonic; and (3) plasma lines (HFPL₂) excited at a frequency 150–250 kHz higher than the pump possibly as a result of the four-wave interaction [14]. The results given by Wu et al. indicated that the four-wave interaction proposed by Borisova et al. cannot quantitatively explain HFPL₂ and that the outshifted plasma line occurred at frequencies slightly above the pump frequency around the reflection altitude of the pump, and the behaviour of the electron temperature and electron density as a function of the pump frequency which was near the fifth electron gyrofrequency [15].

In this article, we present some further research deduced from EISCAT UHF observations during ionospheric heating experiments using the EISCAT heater operated in O-mode polarization and at frequencies sweeping near the fourth electron gyrofrequency on 22 February 2012. Further, we analyze in detail the distinctive features in the behavior of ionospheric plasma parameters, particularly the electron density, electron temperature, HFILs and HFPLs. Finally, we give reasonable explanations for some special phenomena.

2. Experimental Setup

Experiments on the modification of the high-latitude ionosphere were carried out on 22 February 2012, using the EISCAT heater located in Tromsø, Norway (69.6° N, 19.2° E), and this facility radiated high-power, high-frequency O-mode radio waves in the magnetic zenith direction (the antenna pattern is inclined 12° southward from the vertical) at frequencies near $4f_{ce}$ [7]. The EISCAT heater radiated radio waves from the 0th to the 18th and from the 30th to the 48th minute of each hour (18 min heating—12 min pause regime). Phased antenna array No. 1, which had a 7° beam width and an effective radiated power P_{eff} of approximately 600 MW at a frequency of 5.423 MHz, was used in

the experiments. For the first two minutes of each cycle, heating was performed at the frequency $f_{HF} = 5300$ kHz, and then, the frequency f_{HF} increased up to 5600 kHz (by 3.125 kHz every 10 s). In addition, to measure the effect induced by the pump for each step of frequency, the data were analysed using an integration time of 10 s by version 9.0 of GUIDAP (Grand United Incoherent Scatter Design and Analysis Package) software [16] and RTG software (Real Time Graphic). The reliability of the data used in the analysis was confirmed by the value of the residual <2 parameter [16].

During the whole experiment, the earth's magnetic field was in a quiet state, the three-hour K_p indices were 1.5, and the Dst indices were -10 nT. The total magnetic strength on the ground varied in the interval of [53411 nT, 53423 nT] provided by Tromsø Geophysical Observatory, UiT, the Arctic University of Norway at an altitude from 200 km to 250 km and varied in the interval of (48063.9 nT, 49056.6 nT) as calculated by the International Geomagnetic Reference Field (IGRF). Thus, the corresponding fourth electron gyrofrequency at an altitude of 200 km to 250 km should be in the interval of [4382.6 kHz, 49056.6 kHz], which lies exactly in the interval of pump frequency f_{HF} [5.3 MHz, 5.6 MHz]. However, due to the small turbulence in the magnetic field, the fourth electron gyrofrequency will also vary slightly. To facilitate the subsequent description and discussion, it is necessary to divide the pump frequency band into three bands, i.e., a low-frequency band (LB): [5.3 MHz, 5.375 MHz], middle-frequency band (MB): [5.375 MHz, 5.4875 MHz] and high-frequency band (HB): [5.4875 MHz, 5.6 MHz], and each band is six minutes. In fact, Borisova et al. gave the resonant interaction times $t_R = 15:09:10, 15:37:40, \text{ and } 16:06$ UT at frequencies $f_{HF} = 5431, 5400, \text{ and } 5375$ kHz, respectively [7].

The ionosonde in Tromsø received vertical sounding ionograms once every 15 min, Figure 1 shows variations in the critical frequency of F2 layer f_{0F2} (curve a), and these variations were measured by the altitude sounding station in Tromsø from 15:00 to 16:30 UT on 22 February 2012. The calculated upper hybrid frequency $(f_{UH})_{max}$ corresponds to the cut-off frequency of the F2 layer (curve b). The cut-off frequency of the F2 layer was measured by incoherent scattering radar (curve c). Curve d is the pump frequency. At approximately 16:00 (UT), the f_{0F2} values measured by both the ionosonde and incoherent scattering radar are slightly lower than the pump frequency. Therefore, it is safe to say that at the beginning of the third cycle, the heating mode is underdense heating.

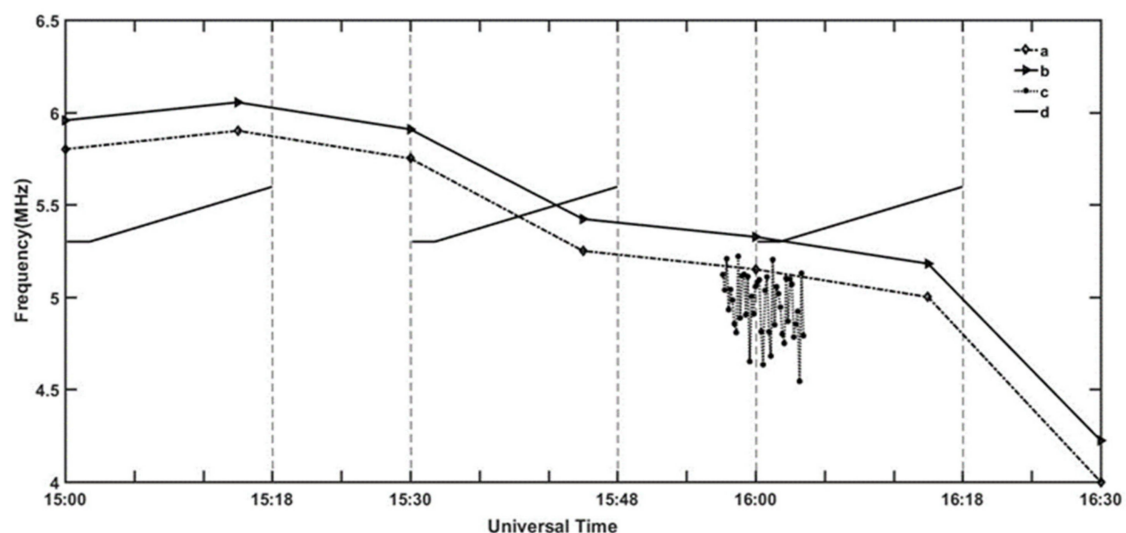


Figure 1. Cut-off frequency (f_{0F2}) measured by the altitude sounding station in Tromsø (curve a) and incoherent scattering radar (curve c), the upper hybrid frequency (curve b) calculated by curve a, and the pump frequency (curve d) corresponding to experiments on 22 February 2012, respectively.

3. Observations

3.1. ISR Spectrum

Figure 2 shows the ion lines at frequencies of -20 kHz to 20 kHz at different altitudes. Since the background electron density profile decreases with time, the heights of the HFILs observed in each cycle are different. The most prominent features are the significant ‘spikes’ in the centre of the ion line spectrum and the significant ‘shoulders’ at ~ 10.7 kHz around the reflection altitude, and these features represent the confirmation of parametric decay instability (PDI) and oscillation two-stream instability (OTSI), respectively [17,18]. In addition, the phenomenon that the altitudes of the HFILs sustained declines in all three cycles, which is also called descending layers (DLs), was also recorded in other heating experiments, i.e., Mishin et al. reported that the enhanced ion line (IL) backscatter from the EISCAT UHF radar descends by 15 – 20 km from the initial interaction altitude [12]. Pedersen et al. used the HAARP ionosonde to reveal that DLs are patches of newly ionized plasma [8,19,20]. Sergeev et al. explored DLs using concurrent measurements of SEE, reflected probing signals, and modular UHF incoherent scatter radar (MUIR) plasma line (PL) backscatter during frequency-stepping experiments at approximately $4f_{ce}$ [9]. The DLs also associated optical emissions at ≈ 732 nm and 427.8 nm (the blue line) indicating electron acceleration above the ionization energies [19,21].

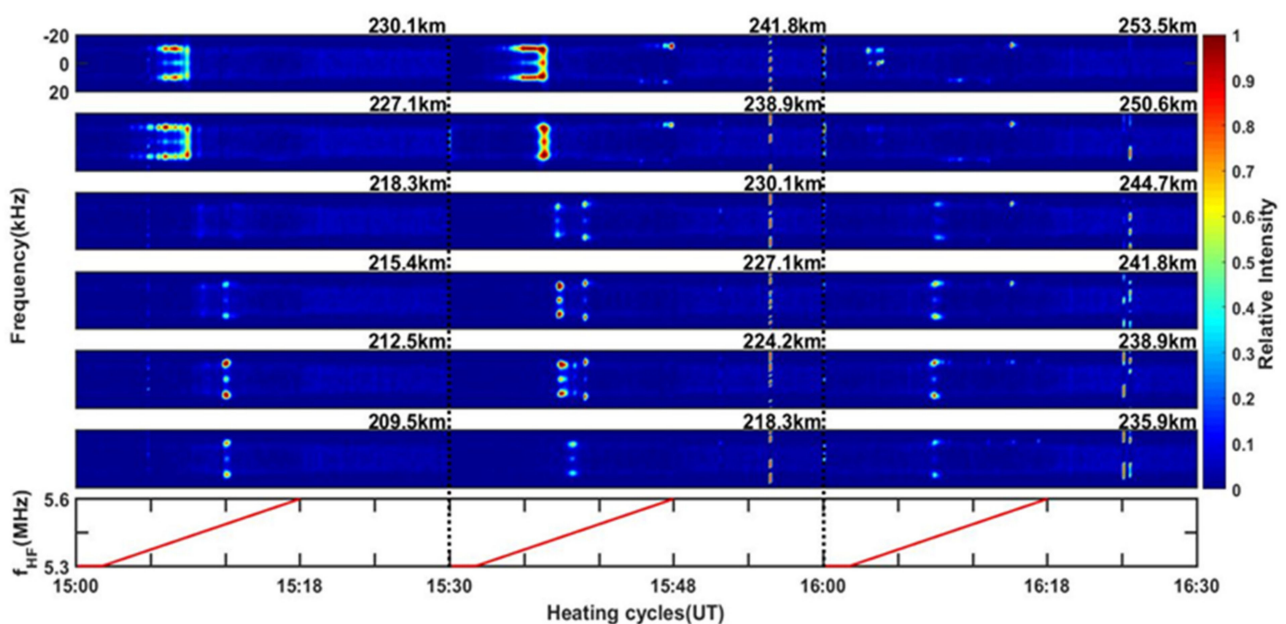


Figure 2. The ion lines from -20 kHz to 20 kHz at different altitudes.

The previous observations at EISCAT showed that the altitude of ion line was about 3 – 5 km higher than the altitude of plasma line [17,18]. Therefore, considering the above altitude difference, the downshifted plasma lines within the frequency range from -5.5 MHz to -6.5 MHz in the altitude range 209.5 – 253.5 km are shown in Figure 3. When recording the HFPLs, the HFPL excitation frequencies f_{HFPL} were close to the pump frequencies of the EISCAT heater [14]. There are some declines in the plasma line spectrum caused by the individual normalization of a plasma line at a particular moment that do not imply a real decrease in the plasma line and any unusual response. We can see from Figure 3 that there are two types of plasma lines; the first is called the ‘decay line’, whose frequency is fulfilled as $f_{HF} - f_{ia}$, from parametric decay instability excited by the pump, where f_{ia} is the frequency of the ion acoustic wave and is ~ 10.7 kHz here. The second type of plasma line shows a frequency upshifted of several hundred kilohertz from the pump frequency and a frequency spread of ~ 70 kHz to ~ 350 kHz. Here we give two examples of the outshifted plasma lines in the first cycle, one is that the enhancement of the plasma-wave

powers at frequencies upshifted from the pump frequency f_{HF} by 350–380 kHz in the MB from 15:05 to 15:09 UT at the altitudes of 221.9 km and 224.9 km, the other is that the enhancement of the plasma-wave powers at frequencies upshifted from the pump frequency f_{HF} by 270–520 kHz in the HB from 15:14 to 15:18 UT at the altitude of 219.0 km. It was also shown the simultaneous excitation of several plasma lines at frequencies close to the pump frequency and at frequencies upshifted by 0.15 to 0.45 MHz for the experiment on 22 February 2012 [22]. This kind of plasma line has also been recorded in [18,23].

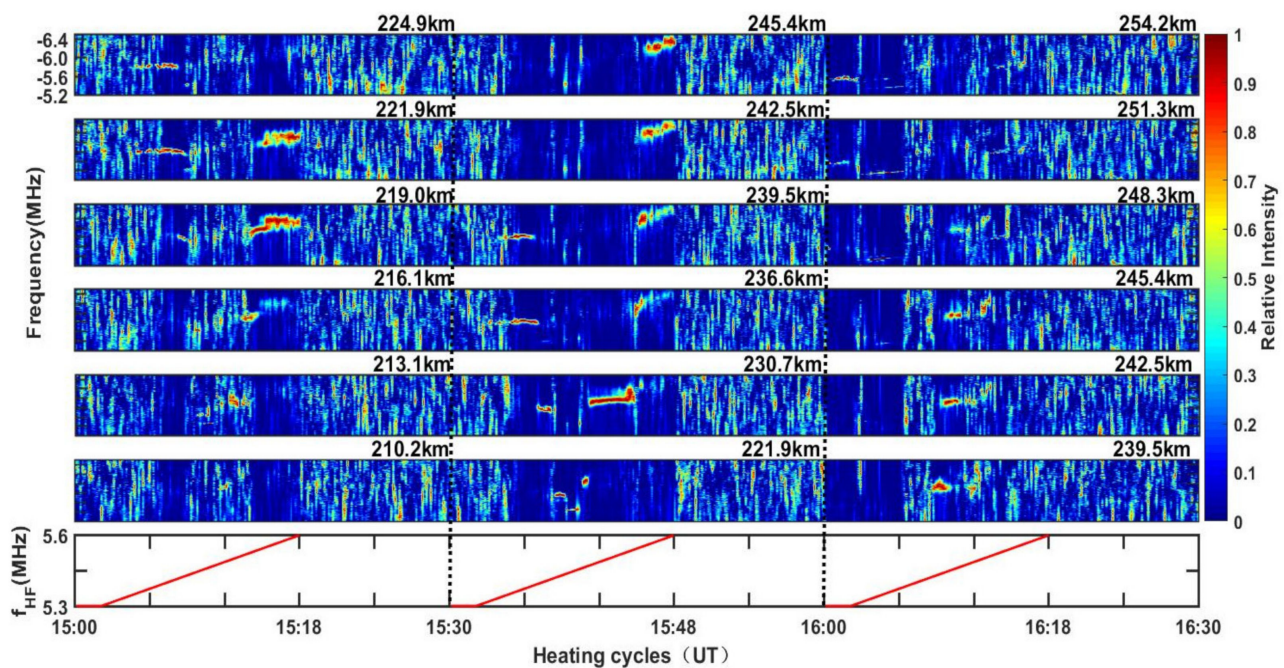


Figure 3. The downshifted plasma lines from -5.5 MHz to -6.5 MHz at different altitudes.

3.2. Electron Temperature

Figure 4 shows that the electron temperature varies with time and altitude. t_R When the heater switched on, some strong enhancements in electron temperature, which appeared independent of altitude and extended up to ~ 500 km, were observed, and when the heater switched off, this kind of enhancement returned to an undisturbed state within 10 seconds. Another significant phenomenon is the enhancement of electron temperature up to 5000 K, which occasionally happened in the MB and HB in the vicinity of the reflection altitude in the second and third cycles. We also found that the strengthening of the electron temperature is suppressed when the pump frequency is in the vicinity of the MB in the third cycle, and this finding is a typical feature in frequency-stepping experiments around nf_{ce} . Moreover, the enhancement of the electron temperature in the LB is less than that in the HB, which is opposite to the result found in the heating frequency near the fifth electron gyrofrequency [15].

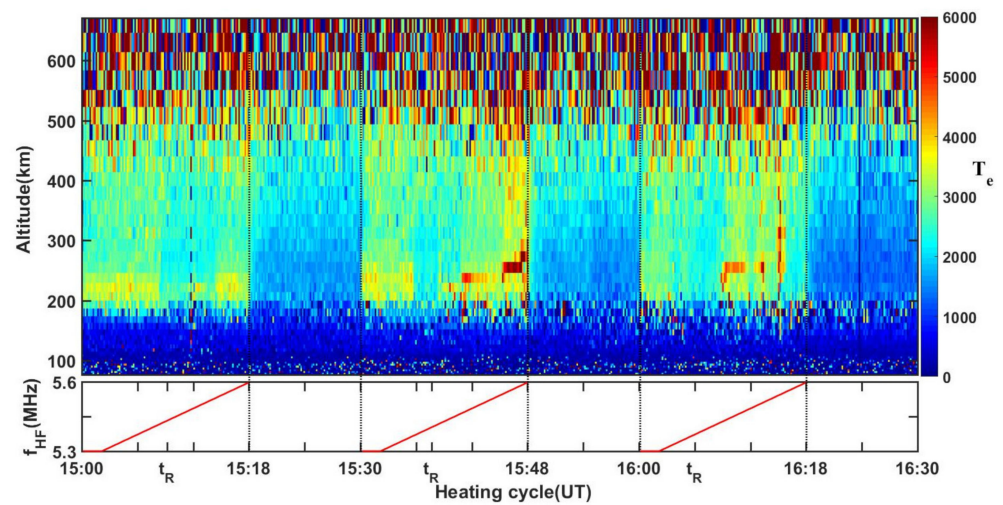


Figure 4. Electron temperature varies with time (t) and altitude (h) when heating.

3.3. Electron Density

Figure 5 shows the variation in the electron density profile during the whole experiment. Comparing the three undisturbed profiles when the heater switched off, we can deduce that the electron density profile decreases with time, which is consistent with the result measured by the altitude sounding station in Tromsø. During heating, the most prominent feature of the electron density is that the electron density increases suddenly up to $\sim 5 \times 10^{11}$, which is consistent with an electron temperature increase up to ~ 5000 K both in time and altitude. Therefore, this enhancement in electron temperature and electron density may be caused by the same mechanism.

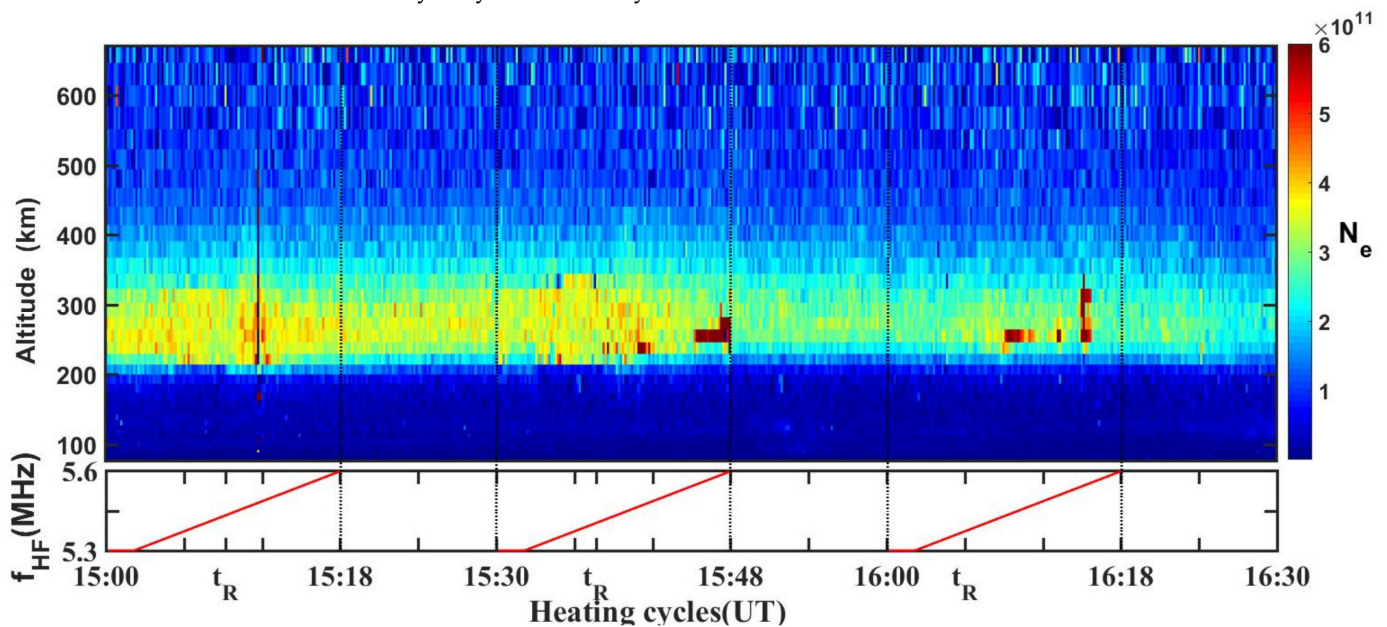


Figure 5. Electron density varies with time (t) and altitude (h) when heating.

4. Discussion

4.1. Plasma Line

In the experiments of high-power HF O-mode radio waves heating the ionosphere, the HFILs and HFPLs, which are caused by PDI and OTSI, can be observed by incoherent scattering radar. Regarding PDI, if the pump wave (ω_0, \vec{k}_0) is strong enough, it can

decay into a Langmuir wave (ω_1, \vec{k}_1) and an ion acoustic wave (ω_2, \vec{k}_2) , where the wave parameters satisfy the matching conditions, $\omega_0 = \omega_1 + \omega_2$ and $\vec{k}_0 = \vec{k}_1 + \vec{k}_2$. Considering that PDI occurs near the reflection height, the vector of the pump wave tends to be zero; hence, $\vec{k}_1 = -\vec{k}_2$. In addition to the OTSI, the pump interacts with a Langmuir wave of equal frequency together with an ion acoustic wave that is spatially period but has zero frequency; namely, $\omega_2 = 0$. In Figure 2, the ‘spike’ in the centre of the ion line spectrum represents the nonshifted maximum in the ion-line spectrum (nonshifted ion line), which indicates the development of oscillation two-stream instability (OTSI). The significant ‘shoulders’ at ~10.7 kHz around the reflection altitude indicate the excitation of ion-acoustic, which is direct indication that parametric decay instability (PDI) develops at altitudes near the reflection of a high-power high-frequency radio wave in the ionosphere [22]. In Figure 3, the first type of plasma line lies at frequency $f_{HF} - 10.7\text{kHz}$ and is caused by PDI. In Figures 2 and 3, the ion lines and plasma lines descend in altitude, and these DLs are patches of newly ionized plasma [8,19,20]. Notably, by comparing Figures 1–3, we find that the HFPLs and HFILs caused by PDI and OTSI are also observed in the third cycle, which is the underdense heating mode. Theoretically, underdense heating is only associated with the wave-particle interaction, and wave-wave interaction cannot occur in this mode; thus, how the PDI and OTSI processes occur in the third cycle is discussed in Section 4.2 in this article.

In Figure 3, the outshifted plasma line, whose frequency is higher than the pump frequency by several hundred kilohertz, cannot be explained by PDI and OTSI, and there are two existing theories trying to explain this phenomenon. The first was proposed by Kuo and Lee [24], who reported that the Langmuir wave (ω_1, \vec{k}_1) , which propagates parallel to the geomagnetic field direction and is generated by PDI excited by the pump near the reflection altitude, scatters into two oblique propagating Langmuir waves (ω_3, \vec{k}_3) and (ω_4, \vec{k}_4) from the background lower hybrid density fluctuations (ω_5, \vec{k}_5) propagating in a direction perpendicular to the magnetic field and generated by parametric excited Langmuir waves near the reflection height [25]; the wave frequency and wave vector match the following conditions:

$$\omega_1 = \omega_3 + \omega_5 = \omega_4 - \omega_5 \quad \vec{k}_1 = \vec{k}_3 + \vec{k}_5 = \vec{k}_4 - \vec{k}_5 \tag{1}$$

where ω_3 and ω_4 correspond to the downshifted and upshifted plasma frequency, respectively; EISCAT UHF radar allows to provide measurements of downshifted plasma line only, so only ω_3 is discussed. If the cascade process of the pump wave occurs several times, the oblique propagating Langmuir waves are superimposed over one another; in this way, the outshifted plasma line may be observed in the plasma spectrum. Considering the Langmuir waves (ω_1, \vec{k}_1) and (ω_3, \vec{k}_3) are observed by the incoherent scattering radar, \vec{k}_1 and \vec{k}_3 should satisfy the radar’s Bragg scattering conditions as follows: $k = |2\vec{k}_r| \approx 39\text{m}^{-1}$, where \vec{k}_r denotes the wave number of the radar wave with a value of 19.6 m^{-1} ; thus, the wave number $\vec{k}_1 = \vec{k}_3$, which implies that $\vec{k}_5 = 0$. Here, we take the observation at 15:42:00 UT in Figure 3 as an example. The reflection altitude was approximately 230 km, and the total magnetic strength was obtained from IGRF by extrapolating the measurements on the ground recorded at 15:42:00 UT by Tromsø Geophysical Observatory, UiT, the Arctic University of Norway at an altitude of 230 km as approximately 48486 nT, so the electron gyrofrequency is $f_{ce} \approx 1.356\text{MHz}$ and the plasma frequency is $f_{pe} \approx 5.889\text{MHz}$. The most common ion species in the F2 layer

is atomic oxygen, but for numerical efficiency, we use the proton-to-electron mass ratio $m_i/m_e \approx 1836$, $f_{ci} \approx 3.4 \times 10^{-5} f_{ce}$, $f_{pi} \approx 0.006 f_{pe}$, and the lower hybrid oscillation frequency $f_{LH} \approx 7.91\text{kHz}$ is obtained by the following formula [26]:

$$f_{LH}^2 = \frac{f_{pi}^2 f_{ce} f_{ci}}{f_{pi}^2 + f_{ce} f_{ci}} \tag{2}$$

where m_i , m_e , f_{ci} and f_{pi} are the ion mass, electron mass, ion gyrofrequency, and ion plasma frequency, respectively. Therefore, it is clear that this theory cannot quantitatively explain the outshifted plasma lines. In addition, the frequency of the outshifted plasma lines slightly increase with the increase of the pump frequency, which can be seen in the MB and HB of the first and second cycle in Figure 3; this finding is contrary to the conclusion given by Kuo and Lee that the amount of upshifted frequency is inversely proportional to the pump frequency [24].

With regard to the parametric decay instability, the pump wave (f_h, \vec{k}_h) decays into a Langmuir wave (f_L, \vec{k}_L) and an ion acoustic wave (f_{ia}, \vec{k}_{ia}) , where the wave parameters satisfy the matching conditions: $f_h = f_L + f_{ia}$, $\vec{k}_h = \vec{k}_L + \vec{k}_{ia}$. Since the pump wave is much longer (order of hundred meters) than the other waves considered (<1 m), \vec{k}_h can be assumed to be ~ 0 , therefore, $\vec{k}_{ia} = -\vec{k}_L = 2\vec{k}_R$, where \vec{k}_R is the radar vector. The Langmuir wave (f_L, \vec{k}_L) excited by PDI will grow continuously, and when it reaches a certain level, it will decay into a new Langmuir wave (f_L^*, \vec{k}_L^*) and an ion acoustic wave $(f_{ia}^*, \vec{k}_{ia}^*)$, since the Langmuir wave (f_L^*, \vec{k}_L^*) can be observed by the radar, so $\vec{k}_L^* = 2\vec{k}_R = -\vec{k}_L$, and $\vec{k}_{ia}^* = \vec{k}_L - \vec{k}_L^* = 2\vec{k}_L$, further, $f_{ia}^* = \left| \vec{k}_{ia}^* C_S \right| = 2f_{ia}$, and thus $f_L^* = f_h - 3f_{ia}^*$. With the same principle, Langmuir wave (f_L^*, \vec{k}_L^*) can act as pump and decay into Langmuir wave $(f_L^{**}, \vec{k}_L^{**})$ and an ion acoustic wave $(f_{ia}^{**}, \vec{k}_{ia}^{**})$, where $f_{ia}^{**} = f_h - 5f_{ia}$. This is called cascade process. Kuo et al. [25,27] reported that the cascade process may play a role in the outshifted plasma lines. This finding also agrees well with the observation shown in Figure 3; that is, taking the second cycle as an example, as the frequency of the pump wave increases, the bandwidth of the spread of the plasma line also increases, as if the higher the pump frequency is, the more the cascade process occurs and further widens the spectrum of the plasma lines.

Another theory involves the strong Langmuir turbulence (SLT) based on the Zakharov model proposed by DuBois et al. [23,28–30]. Near the reflection altitude of the pump wave, if the power of the pump is slightly higher than the threshold of parametric instability, SLT may be excited by the ponderomotive force containing a zero-frequency component. That is, the zero-frequency component of the ponderomotive force can force an electron from a high electric field to regions with a low electric field; thus, a cavity in electron density exists, which can trap Langmuir waves. As the cavity becomes deeper, the pressure gradient of the plasma becomes steeper and compresses the cavity. Finally, the cavity burns out and induces super thermal electrons, which further increase the local electron temperature. In addition, the dispersion relation of the free Langmuir wave is shown below:

$$\omega_f^2 = \omega_{pe}^2 + 3k^2 v_e^2 + (2\pi f_{ce} \sin \alpha)^2 \tag{3}$$

where k is the wave number and α is the angle between the magnetic field and the Langmuir wave. Therefore, the enhancement in local electron temperature can increase the electron

thermal velocity $v_e = 2\sqrt{k_B T_e / m_e}$, further increasing ω_f , where k_B is the Boltzmann constant. Thus, a free Langmuir wave at ω_f that is larger than the pump frequency by an order of several kilohertz may be observed as the outshifted plasma line. Moreover, superimposing the free Langmuir waves from the various altitudes or the altitude integration results in the spread of the plasma line. Here, we also take the observation at 15:42:00 UT in Figure 3 as an example. Because the plasma line is observed by the radar, its wave number should match the relation: $k = \left| 2\vec{k}_r \right| \approx 39m^{-1}$, the electron T_e is approximately 4300 K, and $f_f - f_{HF} \approx 1.653\text{MHz}$ is obtained, where $f_f = \omega_f / 2\pi$. It is obvious that this result does not agree with our observations in Figure 3. In fact, when the wave propagates in a nonuniform plasma medium, its frequency remains constant while its wave number varies with the plasma density, i.e., if the density of the plasma increases, the wave number will decrease, but DuBois et al. neglect the change in the wave number k and argues that the outshifted plasma line is only due to the enhancement in electron temperature.

Mishin et al. proposed that the generation of strong Langmuir turbulence with the oscillating two-stream instability (OTSI) of upper hybrid waves as the primary source of Langmuir waves when f_{0F2} dropped below the pump frequency [31]. At the beginning of the third cycle (which is an underdense heating process), the pump frequency f_{HF} matches the following condition: $f_{0F2} < f_{HF} < (f_{UH})_{\max}$, which means the pump cannot excite Langmuir waves but can excite the upper hybrid resonance, this is the reason why the outshifted plasma line occurs with upper hybrid waves as the primary source of Langmuir waves. In fact, the upper hybrid wave, which propagates perpendicular to the magnetic field, can generate Langmuir waves [32]. The upper hybrid wave $(\omega_{uh}, \vec{k}_{uh})$ can decay into two obliquely propagating Langmuir waves $(\omega_{L1}, \vec{k}_{L1})$ and $(\omega_{L2}, \vec{k}_{L2})$ and an ion mode (ω_s, \vec{k}_s) that is either a purely growing mode or an ion acoustic mode and is parallel to the magnetic field; the frequency and wave vector match the following conditions:

$$\omega_{uh} = \omega_{L1} + \omega_s = \omega_{L2} - \omega_s \text{ and } \vec{k}_{uh} = \vec{k}_{L1} + \vec{k}_s = \vec{k}_{L2} - \vec{k}_s \tag{4}$$

where the Langmuir waves $(\omega_{L1}, \vec{k}_{L1})$ and $(\omega_{L2}, \vec{k}_{L2})$ denote the down-shifted and up-shifted Langmuir waves, respectively. Thus, here, we take $(\omega_{L2}, \vec{k}_{L2})$ into consideration. In addition, Mishin et al. reported that SLT can also develop in upper hybrid altitudes even at low power. First, the above process can excite oblique short-scale Langmuir waves [30]. These waves are transferred into long scales via parametric interactions, e.g., induced scattering on ions. The resulting wave condensate is subjected to modulational instability (also known as OTSI), leading to the SLT regime, albeit weaker than that of the near reflection altitude in the overdense ionosphere.

4.2. Electron Temperature and Electron Density

Comparing Figure 4 with Figure 5, it is clear that there are three distinct variations in electron temperature and electron density as follows: (1) when the heater is operated, both the electron density and electron temperature increase substantially, but the variation in electron density occurs near the reflection altitude of the pump wave, while the enhancement in electron temperature occurs in a wide altitude range from ~200 km to ~500 km. (2) The electron density is synced with the electron temperature increases to three to four times the background value, and this effect can be seen in the MB and HB in the second and third cycles. (3) At the beginning of the third cycle, there is a slight decrease in electron density from ~230 km to ~300 km, and then the electron temperature is enhanced as a function of the pump frequency.

The first type of variation in electron temperature and electron density is the universal phenomenon that occurs in the O-mode heating experiment. During heating, the enhancement in electron temperature is mainly caused by two physical mechanisms. The first is the direct ohmic coupling between the pump and ionospheric plasma, and the second is associated with artificial small-scale irregularities and anomalous absorption [33,34]. Mantas et al. also found the induced enhancement in electron temperature by pump spread over a broader altitude range, for which heat conduction was responsible [35]. Stocker reported that measurements of the electron density revealed both enhancements and depletions in the vicinity of the heater reflection height [36]. These differences are indicative of variations in the balance between the transport and chemical effects.

The second type of variation in electron density and electron temperature occurred only in the second and third cycles, where $f_{HF} > 4f_{ce}$, but not in the first cycle. By comparing Figures 2, 4 and 5, we find another feature of this kind of variation in electron density and electron temperature that is synced with the HFILs. Thus, Langmuir turbulence excited by parametric instability may be responsible for this effect; that is, Langmuir turbulence generated superthermal electrons to exceed the ionization threshold (such ions are O⁺: 13.6 eV and N₂⁺: 15.5 eV) and further increase the electron density. However, in this experiment, the maximum electron temperature is 6700 K at 15:47:40, which corresponds to approximately 0.575 eV; therefore, the heated bulk plasma temperature is not high enough to ionize these species. This finding may be because the incoherent scatter radar is only capable of measuring the electron temperature by assuming a uniform thermal plasma in the scattering volume. Hence, the temperature measurements from radar data in such circumstances would be the weighted average of plasma temperatures within the radar beam. In the first cycle, there is no significant enhancement in the ion line in the HB, so it can be inferred that the parametric decay instability does not occur. This effect may be caused by the pump energy being strongly dissipated by parametric upper hybrid interactions, which further make the pump wave unable to reach the reflection altitude. Therefore, why does this kind of variation only happen in the second and third cycles, rather than the first cycle? The background ionospheric conditions may provide a clue to this question since the only significant difference between the first cycle and the second/third cycles is $f_{0F2} > f_{HF}$.

As for the third type, due to the absence of data in the first and second cycles, we only discuss the third cycle. Figure 1 shows that at the beginning of the third cycle, which is underdense heating, the relationship $f_{0F2} < f_{HF} < (f_{UH})_{max}$ is fulfilled, i.e., the pump wave cannot reach the reflection height, but it can reach the upper hybrid resonance altitude, where the pump can excite the upper hybrid resonance. Therefore, it is reasonable to say that a slight decrease in the electron density should be a result of the trapping of the upper hybrid wave excited by the pump at the upper hybrid resonance altitude [4]. During heating, the O-mode pump can couple into an upper hybrid wave at the upper hybrid resonance altitude through either a pre-existing or artificially induced irregularity [4,37,38], and the pump matches the following condition:

$$f_{HF} = f_{UH} = \sqrt{f_{pe}^2 + f_{ce}^2} \quad (5)$$

where f_{UH} is the upper hybrid frequency. That is, at the upper hybrid resonance altitude, the pump may excite the upper hybrid resonance in the background ionosphere, which may be linearly converted into the upper hybrid wave at the edge of the irregularity and propagate into the irregularity along the gradient of electron density. Then, the upper hybrid wave propagates in a direction perpendicular to the magnetic field and dissipates energy through ohmic loss. Furthermore, this wave heats electrons and finally leads to an effect of reducing the electron density due to thermal electron transport. Hence, at the beginning of the third cycle, a slight decrease in electron density and an enhancement in electron temperature were observed. As the pump frequency increases near the fourth electron gyrofrequency, the electron temperature begins to decrease, and when $f_{HF} > 4f_{ce}$, the electron temperature increases again. This result is a typical feature of the electron

temperature variation with the pump frequency near the gyrofrequency recorded by Borisova et al. and Wu Jun et al., and this phenomenon is related to the second cut-off frequency in the upper hybrid dispersion relation [7,14,15].

Here, we assume an individual small-scale irregularity with constant initial electron density N_1 , whose upper hybrid frequency is ω_{UH}^1 and second cut-off frequency is ω_{max}^1 [4], and the background ionospheric plasma N_0 has the upper hybrid frequency ω_{UH}^0 . Because the electron density decrease at the beginning of the third cycle, it is reasonable to assume that $N_1 < N_0$ and further that $\omega_{UH}^1 < \omega_{UH}^0$. When the pump is operated at a particular frequency between ω_{UH}^1 and ω_{max}^1 , the upper hybrid resonance ω_{UH}^1 will be excited in N_0 . At the edge of N_1 , those upper hybrid resonances will be linearly converted into the upper hybrid wave and propagate into N_1 and be trapped by N_1 , furthermore, this wave dissipates energy through ohmic loss and heats electrons in N_1 , and the escape of thermal electrons from N_1 will make the electron density of N_1 further decrease [15]. When the pump is operated at a higher frequency that is closer to the fourth gyrofrequency, the upper hybrid wave excited by the pump in N_0 is reflected on the surface of N_1 and cannot propagate into N_1 . Thus, upper hybrid waves will not be trapped in N_1 , and N_1 will not grow. When the pump frequency is higher than the fourth gyrofrequency, the dispersion curve of the upper hybrid wave in N_0 almost coincides with that of the fourth harmonic of the Bernstein wave in N_1 for a small wave number; thus, the trapping of the upper hybrid wave should be poor.

In addition, the existence of a second cut-off in the upper hybrid dispersion relation may provide an explanation for the question proposed in the first paragraph in Section 4.1; this explanation describes why the plasma line and ion line generated by PDI and OTSI were observed during underdense heating in the third cycle. That is, at the beginning of the third cycle, a small-scale irregularity traps the upper hybrid wave and dissipates its energy to heat the electron. When the pump frequency is near the fourth gyrofrequency, the heating in the electron should be suppressed due to the second cut-off frequency, which means that the electron density will increase due to the thermal pressure and further makes the ionospheric critical frequency increase so that the pump frequency may be temporarily below the critical frequency of the ionosphere. In this situation, the PDI and OSTI may be excited by the pump, which provides a necessary condition to generate SLT.

5. Conclusions

This paper reports experimental observations from pumping near the fourth electron gyrofrequency on 22 February 2012 at the EISCAT Tromsø site in northern Norway.

The outshifted plasma lines around the reflection altitude of the pump at frequencies several hundred kilohertz above the pump frequency were observed by the UHF incoherent scatter radar, and the results of analysis indicate that both Langmuir wave scattering off the lower hybrid density fluctuations and SLT in the Zakharov model suggested by Kuo et al. and DuBois et al., respectively, cannot quantitatively explain the outshifted plasma lines [23,24,28–30]. The observations are contrary to the conclusion given by Kuo and Lee that the amount of up-shifted frequencies is inversely proportional to the pump frequency. However, they advocated another idea that the cascade process plays an important role in the outshifted plasma lines, which agrees well with the observations in this experiment [24]. In addition, at the beginning of the third cycle, when the pump frequency matches the relation $f_{0F2} < f_{HF} < (f_{UH})_{max}$, which indicates that the pump cannot excite the Langmuir wave, the theory in this situation is that the upper hybrid wave can decay into two obliquely propagating Langmuir waves, and an ion mode advocated by Kuo et al. can generate the source of the Langmuir wave for the outshifted plasma lines [31].

The spatiotemporal consistency between the enhancement in electron density /electron temperature is three to four times that of the undisturbed state and HFILs suggest that SLT excited by parametric instability plays a significant role in superthermal electron formation and electron acceleration.

Furthermore, we first propose that some enhancements in HFILs and HFPLs generated by parametric decay instability (PDI) during underdense heating in the third cycle are due to the existence of a second cut-off frequency in the upper hybrid dispersion relation as derived from a kinetic description.

Author Contributions: Investigation, Z.L.; writing—original draft preparation, Z.L. and H.F.; writing—review and editing, Z.L.; supervision, H.G. and Z.G. All authors have read and agreed to the published version of the manuscript.

Funding: This research was funded by the National Natural Science Foundation of China (grant number 41804149) and China Scholarship Council.

Data Availability Statement: Publicly available datasets were analyzed in this study. This data can be found here: [<https://www.eiscat.se/schedule/schedule.cgi> and <http://flux.phys.uit.no/geomag.html>] (accessed on 6 June 2021).

Acknowledgments: EISCAT is an international scientific association supported by research organizations in China (CRIRP), Finland (SA), Japan (NIPR and STEL), Norway (NFR), Sweden (VR), and the United Kingdom (NERC). The experiments reported in this paper was carried out by the Russian team leading by Borisova. The authors are grateful to the EISCAT for providing the diagnostic data of the heating experiment on 22 February 2012 and Tromsø Geophysical Observatory, UiT, the Arctic University of Norway for providing the magnetic data for Tromsø recorded on 22 February 2012, which can obtain from <https://www.eiscat.se/schedule/schedule.cgi> and <http://flux.phys.uit.no/geomag.html>, respectively (accessed on 6 June 2021).

Conflicts of Interest: The authors declare no conflict of interest.

References

- Gurevich, A.V. Nonlinear effects in the ionosphere. *Phys. Usp.* **2007**, *50*, 1091. [[CrossRef](#)]
- Frolov, V.L.; Bakhmet'eva, N.V.; Belikovich, V.V.; Vertogradov, G.G.; Vertogradov, V.G.; Komrakov, G.P.; Kotik, D.S.; Mityakov Nikolai, A.; Polyakov, S.V.; Rapoport, V.O. Modification of the earth's ionosphere by high-power high-frequency radio waves. *Phys. Usp.* **2007**, *50*, 315–324. [[CrossRef](#)]
- Brodin, G.; Stenflo, L. A new decay channel for upper-hybrid waves. *Phys. Scr.* **2016**, *91*, 104005. [[CrossRef](#)]
- Mjølhus, E. On the small scale striation effect in ionospheric radio modification experiments near harmonics of the electron gyro frequency. *J. Atmos. Terr. Phys.* **1993**, *55*, 907–918. [[CrossRef](#)]
- Honary, F.; Stocker, A.J.; Robinson, T.R.; Jones, T.B.; Stubbe, P. Ionospheric plasma response to HF radio waves operating at frequencies close to the third harmonic of the electron gyrofrequency. *J. Geophys. Res. Space Phys.* **1995**, *100*, 21489–21501. [[CrossRef](#)]
- Robinson, T.R.; Honary, F.; Stocker, A.J.; Jones, T.B.; Stubbe, P. First EISCAT observations of the modification of F-region electron temperature during RF heating at harmonics of the electron gyro-frequency. *J. Atmos. Terr. Phys.* **1996**, *58*, 385–395. [[CrossRef](#)]
- Borisova, T.D.; Blagoveshchenskaya, N.F.; Kalishin, A.S.; Kosch, M.; Senior, A.; Rietveld, M.T.; Yeoman, T.K.; Hagstrom, I. Phenomena in the high-latitude ionospheric F region induced by a HF heater wave at frequencies near the fourth electron gyroharmonic. *Radiophys. Quantum Electron.* **2014**, *57*, 1–19. [[CrossRef](#)]
- Pedersen, T.; Gustavsson, B.; Mishin, E.; Kendall, E.; Mills, T.; Carlson, H.C.; Snyder, A.L. Creation of artificial ionospheric layers using high-power HF waves. *Geophys. Res. Lett.* **2010**, *37*, 211–228. [[CrossRef](#)]
- Sergeev, E.; Grach, S.; Shindin, A.; Mishin, E.; Bernhardt, P.; Briczinski, S.; Isham, B.; Broughton, M.; Labelle, J.; Watkins, B. Artificial Ionospheric Layers during Pump Frequency Stepping Near the 4th Gyroharmonic at HAARP. *Phys. Rev. Lett.* **2013**, *110*, 065002. [[CrossRef](#)] [[PubMed](#)]
- Dhillon, R.S.; Robinson, T.R. Observations of time dependence and aspect sensitivity of regions of enhanced UHF backscatter associated with RF heating. *Ann. Geophys.* **2005**, *23*, 75–85. [[CrossRef](#)]
- Ashrafi, M.; Kosch, M.J.; Kaila, K.; Isham, B. Spatiotemporal evolution of radio wave pump-induced ionospheric phenomena near the fourth electron gyroharmonic. *J. Geophys. Res. Space Phys.* **2007**, *112*, 05314. [[CrossRef](#)]
- Mishin, E.; Watkins, B.; Lehtinen, N.; Eliasson, B.; Pedersen, T.; Grach, S. Artificial ionospheric layers driven by high-frequency radio waves: An assessment. *J. Geophys. Res. Space Phys.* **2016**, *121*, 3497–3524. [[CrossRef](#)]
- Kuo, S.P. Electron cyclotron harmonic resonances in high-frequency heating of the ionosphere. *Phys. Plasma* **2013**, *20*, 092124. [[CrossRef](#)]
- Borisova, T.D.; Blagoveshchenskaya, N.F.; Kalishin, A.S.; Rietveld, M.T.; Yeoman, T.K.; Hågström, I. Modification of the high-latitude ionospheric F region by high-power HF radio waves at frequencies near the fifth and sixth electron gyroharmonics. *Radiophys. Quantum Electron.* **2016**, *58*, 561–585. [[CrossRef](#)]

15. Wu, J.; Wu, J.; Rietveld, M.T.; Haggstrom, I.; Zhao, H.; Xu, Z. The behavior of electron density and temperature during ionospheric heating near the fifth electron gyrofrequency. *J. Geophys. Res. Space Phys.* **2017**, *122*, 1277–1295. [[CrossRef](#)]
16. Lehtinen, M.S.; Huuskonen, A. General incoherent scatter analysis and GUIDAP. *J. Atmos. Terr. Phys.* **1996**, *58*, 435–452. [[CrossRef](#)]
17. Stubbe, P.; Kohl, H.; Rietveld, M.T. Langmuir turbulence and ionospheric modification. *J. Geophys. Res. Space Phys.* **1992**, *97*, 6285–6297. [[CrossRef](#)]
18. Kohl, H.; Kopka, H.; Stubbe, P.; Rietveld, M.T. Introduction to ionospheric heating experiments at Tromsø-II. Scientific problems. *J. Atmos. Terr. Phys.* **1993**, *55*, 601–613. [[CrossRef](#)]
19. Pedersen, T.; Gustavsson, B.; Mishin, E. Optical ring formation and ionization production in high-power HF heating experiments at HAARP. *Geophys. Res. Lett.* **2009**, *36*, L18107. [[CrossRef](#)]
20. Pedersen, T.; Gustavsson, B.; Mishin, E. Production of artificial ionospheric layers by frequency sweeping near the 2nd gyroharmonic. *Ann. Geophys.* **2011**, *29*, 47–51. [[CrossRef](#)]
21. Hysell, D.L.; Miceli, R.J.; Kendall, E.A.; Schlatter, N.M.; Varney, R.H.; Watkins, B.J.; Pedersen, T.R.; Bernhardt, P.A.; Huba, J.D. Heater-induced ionization inferred from spectrometric airglow measurements. *J. Geophys. Res. Space Phys.* **2014**, *119*, 2038–2045. [[CrossRef](#)]
22. Borisova, T.D.; Blagoveshchenskaya, N.F.; Rietveld, M.T.; Häggström, I. Outshifted Plasma Lines Observed in Heating Experiments in the High-Latitude Ionosphere at Pump Frequencies Near Electron Gyroharmonics. *Radiophys. Quantum Electron.* **2019**, *61*, 722–740. [[CrossRef](#)]
23. Dubois, D.F.; Rose, H.; Russell, D. Power spectra of fluctuations in strong Langmuir turbulence. *Phys. Rev. Lett.* **1988**, *61*, 2209–2212. [[CrossRef](#)] [[PubMed](#)]
24. Kuo, S.P.; Lee, M.C. A source mechanism producing HF-induced plasma lines (HFPLS) with up-shifted frequencies. *Geophys. Res. Lett.* **1992**, *19*, 249–252. [[CrossRef](#)]
25. Kuo, S.P.; Lee, M.C. On the generation of a broad downshifted spectrum of HF wave enhanced plasma lines in the ionospheric heating experiments. *Geophys. Res. Lett.* **1999**, *26*, 3289–3292. [[CrossRef](#)]
26. Najmi, A.; Eliasson, B.; Shao, X.; Milikh, G.M.; Papadopoulos, K. Simulations of ionospheric turbulence produced by HF heating near the upper hybrid layer. *Radio Sci.* **2016**, *51*, 704–717. [[CrossRef](#)]
27. Kuo, S.P. Cascade of the parametric decay instability in ionospheric heating experiments. *J. Geophys. Res. Space Phys.* **2001**, *106*, 5593–5597. [[CrossRef](#)]
28. Dubois, D.F.; Rose, H.; Russell, D. Excitation of strong Langmuir turbulence in plasmas near critical density: Application to HF heating of the ionosphere. *J. Geophys. Res. Space Phys.* **1990**, *95*, 21221–21272. [[CrossRef](#)]
29. Dubois, D.F.; Rose, H.; Russell, D. Coexistence of parametric decay cascades and caviton collapse at subcritical densities. *Phys. Rev. Lett.* **1991**, *66*, 1970–1973. [[CrossRef](#)]
30. Dubois, D.F.; Hanssen, F.; Rose, H. Space and time distribution of HF excited Langmuir turbulence in the ionosphere: Comparison of theory and experiment. *J. Geophys. Res. Space Phys.* **1993**, *98*, 17543–17567. [[CrossRef](#)]
31. Mishin, E.; Burke, W.; Pedersen, T. On the onset of HF-induced airglow at HAARP. *J. Geophys. Res. Space Phys.* **2004**, *109*, A02305. [[CrossRef](#)]
32. Kuo, S.; Lee, M.; Kossey, P. Excitation of oscillating two-stream instability by upper hybrid pump in ionospheric heating experiments at Tromsø. *Geophys. Res. Lett.* **1997**, *24*, 2969–2972. [[CrossRef](#)]
33. Utlaut WF Violette, E.J. A summary of vertical incidence radio observations of ionospheric modification. *Radio Sci.* **1974**, *9*, 895–903. [[CrossRef](#)]
34. Gurevich, A.V.; Lukyanov, A.V.; Zybin, K.P. Anomalous absorption of powerful radio waves on the striations developed during ionospheric modification. *Phys. Lett. A* **1996**, *211*, 363–372. [[CrossRef](#)]
35. Mantas, G.P.; Carlson, H.C.; LaHoz, C.H. Thermal response of the F region ionosphere in artificial modification experiments by HF radio waves. *J. Geophys. Res. Space Phys.* **1981**, *86*, 561–574.
36. Stocker, A.J.; Honary, F.; Robinson, T.R.; Jones, T.B.; Stubbe, P.; Kopka, H. EISCAT observations of large-scale electron temperature and electron density perturbations caused by high power HF radio waves. *J. Atmos. Terr. Phys.* **1992**, *54*, 1555. [[CrossRef](#)]
37. Dysthe, K.B.; Mjølhus, E.; Pécseli, H. Thermal cavitons. *Phys. Scr.* **1982**, *1982*, 548. [[CrossRef](#)]
38. Rietveld, M.T.; Kosch, M.J.; Blagoveshchenskaya, N.F.; Kornienko, V.A.; Leyser, T.B.; Yeoman, T.K. Ionospheric electron heating, optical emissions, and striations induced by powerful HF radio waves at high latitudes: Aspect angle dependence. *J. Geophys. Res. Space Phys.* **2003**, *108*, 1141–1156. [[CrossRef](#)]